Modifications of unpromoted and cobalt-promoted MoS_2 during thermal treatment by dimethylsulfide

Gilles Berhault [a,*], Leonel Cota Araiza [b], Alberto Duarte Moller [b], Apurva Mehta [c], and Russell R. Chianelli [d,*]

[a] *Laboratoire de Catalyse en Chimie Organique, UMR6503-CNRS, Université de Poitiers, 40, avenue du Recteur Pineau, 86022 Poitiers Cedex France*
[b] *Centro de Ciencias de la Materia Condensada (CCMC), Apartado postal 2681, 22830, Ensenada, BC, México; PO Box 439036, San Ysidro, CA, 92143, USA*
[c] *Stanford Synchrotron Radiation Laboratory, Stanford University, SLAC, Stanford, CA, 94309, USA*
[d] *University of Texas at El Paso, Materials Research and Technology Institute, El Paso, TX, 79968, USA*

Received 21 June 2001; accepted 26 September 2001

Previous results have shown that the active surface in stabilized active sulfide catalysts is carbided. This fact led us to reconsider the influence of organosulfide agents in the activation of hydrotreatment catalysts. Structural and morphological consequences of dimethylsulfide treatment of (Co)/MoS_2-based solids were studied. Results suggest that the electronic promotion of Mo by Co substantially influences the carbon replacement of sulfur atoms at the edges of molybdenum sulfide layers.

KEY WORDS: MoS_2; MoS_xC_y; CoMoS; CoMoC; hydrodesulfurization; dimethylsulfide

1. Introduction

Hydrotreating processes are used extensively in refineries to improve the environmental quality of liquid transportation fuels. Elevated temperatures (573–673 K) and high hydrogen pressures are required in this catalytic process to carry out hydrogenolysis reactions of C–S, C–N, C–O or C–metal bonds [1]. Catalysts used to perform these reactions are sulfide catalysts, particularly molybdenum or tungsten sulfides supported on alumina and promoted by cobalt or nickel. Since the seventies, many studies were made in order to understand the nature of the Co or Ni synergetic effect on molybdenum sulfide. The first detailed model describing electronic promotion was proposed by Voorhoeve and Stuiver [2] and Farragher and Cossee [3]. In this model, the promotion effect was the result of a charge transfer from pseudo-intercalated Ni promoting atoms to W^{4+} creating W^{3+} sites. The first evidence of a particular Co environment was demonstrated through studies performed by Topsøe *et al.* [4]. They showed the existence of the so-called "CoMoS" phase in which Co atoms were located at the edges of MoS_2 crystallites in a "decoration" mode. The existence of the "CoMoS" as a "precursor" phase is well established. However, recent results have shown that, in real hydrotreating conditions (triphasic reactor with a liquid phase made of a complex mixture of hydrocarbons leading to a very high partial pressure of "carbon" compounds), the stabilized active phase contains structurally important amounts of carbon which up to this point has been largely ignored [5]. Early evidence of a carbidic nature of the active phase was found in the patents of Chianelli and Pecoraro [6,7] and of Seiver and Chianelli [8]. More recent studies have confirmed this initial observation showing that the final stoichiometry of the active phase should be viewed as MoS_yC_z with carbon replacing some sulfur atoms on the edges of the molybdenum sulfide hexagonal lattice.

This final "carbosulfide" surface state can be obtained through different methods. Firstly, this stabilized phase was prepared after catalyzing the desulfurization of dibenzothiophene in a decalin carrier with usual hydrotreatment conditions (350 °C, 35 atm H_2) using a Carberry reactor [5]. This MoS_yC_z stoichiometry could also be obtained through the decomposition of a tetraalkylthiometallate precursor, *i.e.*, $(NR_4)_2MeS_4$ (Me = Mo, W) [9,10]. Finally, in a previous study, Berhault *et al.* [11] have shown that the interaction of dimethylsulfide (DMS) with an unsupported molybdenum sulfide catalyst could equally achieve a MoS_yC_z final stoichiometry. Using bulk and surface techniques and molecular simulations as well, they were able to characterize the structural and morphological consequences of the DMS–MoS_2 interaction. While the bulk phase stays sulfidic by nature, the surface presents a carbidic character with carbon replacing surface sulfur atoms. The initial MoS_{2+x} stoichiometry gives rise to a final MoS_yC_z phase with $y + z = 2 + x$ in the presence of a hydrogen atmosphere while excess carbon is present if the DMS treatment is performed under a nitrogen atmosphere. Apart from this structural modification, morphological consequences are also observed with the formation of better dispersed crystallites after the DMS treatment particularly when a nitrogen atmosphere is used. These results led us to reconsider the role of carbon in hydrotreating applications, mainly the activation of sulfide catalysts by organosulfide agents (dimethylsulfide, dimethyldisulfide, alkylpolysulfides, *etc.*). Indeed, it is well known that acti-

* To whom correspondence should be addressed. E-mail: Gilles.Berhault@univ-poitiers.fr; Chianell@utep.edu

1011-372X/02/0300-0081/0

vation by carbon-containing sulfiding agents enhances the hydrodesulfurization (HDS) activity [12–14]. It should also be mentioned that, if one starts with a bulk carbide catalyst, the active phase in the presence of sulfur reactants tends to a carbosulfide surface phase similar to the one observed in sulfide catalysts [15,16].

The objective of this work is to give an overview of the structural modifications of both unpromoted and cobalt-promoted MoS_2 phases with particular attention to the influence of the promotion over the degree of carburization of the initial MoS_2 system. A tentative model is presented in order to explain the C–S exchange on the surface of MoS_2 catalysts and the morphological consequences inherent to this carbon inclusion.

2. Experimental

2.1. Catalyst preparation

2.1.1. Synthesis of the $(NH_4)_2MoS_4$ and $Co/(NH_4)_2MoS_4$ precursors

The $(NH_4)_2MoS_4$ precursor was readily prepared by adding $(NH_4)_2S$, 42.5% in aqueous solution to $(NH_4)_6[Mo_7O_{24}]\cdot 4H_2O$ diluted in a minimal amount of water. This preparation has been described previously [11]. For the cobalt-containing precursor, $CoCl_2\cdot 6H_2O$ was added to the red orange solution of $(NH_4)_2MoS_4$ in the atomic proportion, $Co/(Co + Mo) = 0.3$. Immediately, a black precipitate is formed. The precipitate was washed several times with isopropanol before drying on a vacuum filter.

2.1.2. Thermal decomposition of $Co/(NH_4)_2MoS_4$ into Co/MoS_{2+x}

The precursor was thermally decomposed under N_2 at a given temperature for 2 h (heating rate 2.5 K min^{-1}, N_2 flow 60 cm^3 min^{-1}). The temperature of the thermal treatment was modified to vary the S/Mo ratio. At temperatures higher than 573 K, MoS_{2+x} was obtained through decomposition of MoS_3 (the value of x decreases with increasing temperature until pure MoS_2 is obtained). After this treatment, the solids were cooled down to room temperature (RT) under N_2 and stored in sealed bottles. MoS_2 and Co/MoS_2 samples were labeled MST or CMST with T, temperature of N_2 treatment in K.

2.1.3. Dimethylsulfide thermal treatment

MoS_{2+x} samples (100 mg) were flushed under N_2 at RT for 15 min before being contacted with a mixture of CH_3–S–CH_3 (DMS) diluted in N_2 or H_2. The DMS partial pressure was fixed at 180 Torr (24.0 kPa). The solids were then heated under this flowing reactant mixture up to a given temperature (573 K $< T <$ 833 K) at a heating rate of 2.5 K min^{-1} and maintained at this temperature for 1 h. The samples were then cooled to RT in the presence of the N_2 (H_2)/CH_3–S–CH_3 mixture, flushed for 2 h with N_2 and stored in sealed bottles under Ar. Elemental analyses (Mo, S and C contents) were performed by Galbraith Laboratories, Inc. Sulfur content overestimation was corrected using a crystalline MoS_2 sample (MoS_2 single crystal from Climax Molybdenum, Inc.) as a reference.

2.2. FTIR spectroscopy

The samples were characterized by infrared spectroscopy in the 4000–200 cm^{-1} wavenumber range. Samples were prepared by dilution in CsI powder (Wilmad, Infrared Grade) in a 1% mass ratio. CsI powder was preferred due to its high transparency in the far-infrared region until 180 cm^{-1}. The IR spectra were recorded using an ATI Mattson Infinity 60 AR spectrometer. The far-infrared domain (<500 cm^{-1}) as well as the mid-IR region was inspected with a DTGS detector equipped with a PE window (far-IR) and a CsI beamsplitter. Spectra were then recorded in the 2000–180 cm^{-1} region, for higher wavenumber domains, acquisitions were carried out by switching to a KBr beamsplitter. Band intensities were corrected for slight differences in weight. Spectra treatment was carried out using the IR Winfirst software. FTIR spectroscopy was used either to characterize MoS_2 samples treated in a flow reactor in the presence of CH_3–S–CH_3 or to prepare directly *in situ* carbided MoS_2 samples. This alternative preparation was made by heating a 1% MoS_2/CsI pellet in the presence of 10 Torr of DMS. The KBr window-equipped cell was previously evacuated at RT before contact with DMS. The pellet was then heated to a given temperature at 2.0 K min^{-1} and maintained at this temperature for 1 h. The sample was then cooled down until RT in the presence of CH_3–S–CH_3 and then evacuated for 2 h. Spectra were then recorded without any contact with air.

2.3. Synchrotron X-ray diffraction

Synchrotron XRD experiments were performed at the Stanford Synchrotron Radiation Laboratory on beamline 2-1. The high brightness and vertical collimation of the synchrotron beam allow use of a Si(111)-based detector able to resolve lattice parameter changes of the order of 0.1%. The size of the focused beam is 2 × 1 mm and approximately 10^{11} photons/s are incident on the sample at an energy of 1.0×10^4 eV ($\lambda = 1.2389$ Å). The XRD patterns were collected in the 4°–104° 2θ range with an increment of 0.1°. The synchrotron source was used to determine structural differences before and after the carbiding process under a nitrogen atmosphere. A higher temperature of treatment (833 K) than normally present in hydrotreating conditions is used in order to emphasize the interaction of the DMS treatment with the molybdenum disulfide phase.

2.4. Electron energy loss spectroscopy

The samples were ultrasonically dispersed in ethanol. A drop of the suspension was then placed in a holey carbon

Cu grid. The observations were performed with a Jeol 2010 transmission electron microscope equipped with a Gatan 666 parallel spectrometer. Attention was devoted to the vicinity of the C K-edge transition region around 300 eV.

2.5. Molecular simulations

The *Crystal Builder, Surface Builder, Interface Builder, Force-Field, IR/Raman, Diffraction Crystal and Rietveld (DBWS)* modules of the Cerius^2 4.0 simulation package of Molecular Simulation Inc. (MSI) were used to compare experimental XRD and IR results with a theoretical model of the structure and stability of bulk MoS_2. The crystalline models were generated using the *Crystal Builder* module (MoS_2 atomic positions, symmetry conditions and lattice parameters). The minimum energy configuration was calculated using a force–field Westheimer method based on the Born–Openheimer approximation.

3. Results

Unsupported MoS_2 catalysts were prepared by decomposition of ATTM (ammonium tetrathiomolybdate, $(NH_4)_2MoS_4$) under an inert gas. The thermal decomposition of ATTM was chosen for preparation of samples because this method provides a simple and reproducible method for preparing pure MoS_2 catalysts. Careful heating of the ATTM precursor at increasing temperatures in a N_2 atmosphere produces MoS_{2+x} bulk solids with x representing excess sulfur in the catalyst presumably located at the edges [5]. Figure 1 reports the variation of the overstoichiometric S/Mo ratio (called x) with increasing temperature of treatment. Large S/Mo variations can be obtained using this procedure with x varying from 0.0 to 0.5. Stoichiometric MoS_2 is progressively obtained as the excess sulfur and the edge area are vanishing. The thermal decomposition of the $(NH_4)_2MoS_4$ precursor was carefully followed in order to accurately evaluate the morphological changes due to the DMS treatment described later in this report.

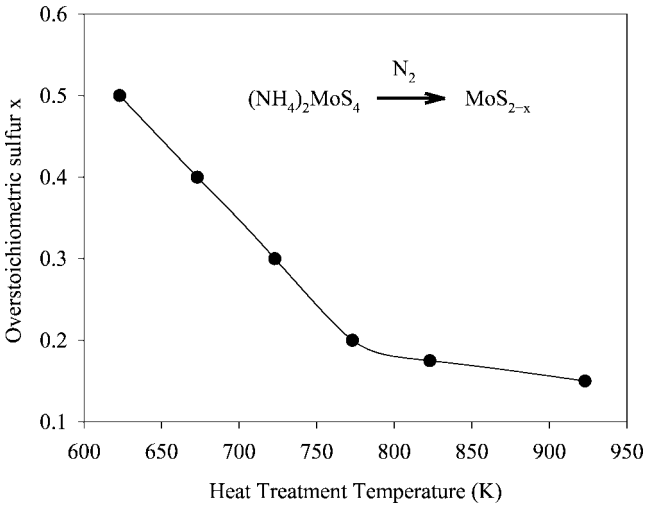

Figure 1. Variation of the overstoichiometric S/Mo ratio x of a typical MoS_{2+x} sample prepared from $(NH_4)_2MoS_4$ (ATTM) precursor in the presence of a N_2 mixture.

3.1. Infrared spectroscopy

Figure 2 reports the evolution of the IR bands in the range 600–200 cm^{-1} for different temperatures of treatment under N_2. The MoS_2 sample obtained by ATTM thermal decomposition at 573 K (MS573) presents very weak bands at 385, 468 and 530 cm^{-1}. Increasing the temperature about 30 K causes an increase of the 385 and 467 cm^{-1} band while the 530 cm^{-1} signal stays relatively constant. The 385 and 467 cm^{-1} signals are assigned to the Mo–S stretching modes of vibrations, respectively, along the basal plane ($E \perp c$, 385 cm^{-1}) and perpendicularly to the basal plane ($E \parallel c$, 467 cm^{-1}) [17]. Treatment at higher temperatures ($T > 773$ K) is associated with increasing and sharpening of the two ν(Mo–S) modes while the 530 cm^{-1} broad band progressively vanishes. This signal is ascribed to $(S–S)^{2-}$ bands coming from the linking of small MoS_2 slabs, which are located at the edges [18]. For cobalt-promoted MoS_2 phase, spectra were oversimplified and the Mo–S stretching bands generally appeared very weak, as observed by Schrader and Cheng [19]. The absence of a broad profile centered on 330 cm^{-1} even at 573 K suggests that the amorphous MoS_3 phase has already been decomposed at this temperature and the MoS_2 local structure is emerging [20]. Moreover, the increase of temperature enhances more strongly the 385 cm^{-1} intensity peak than the 467 cm^{-1} one. This effect could be related to a more rapid increase of the stacking number of the MoS_2 layered structure compared to the particle growth along the basal plane.

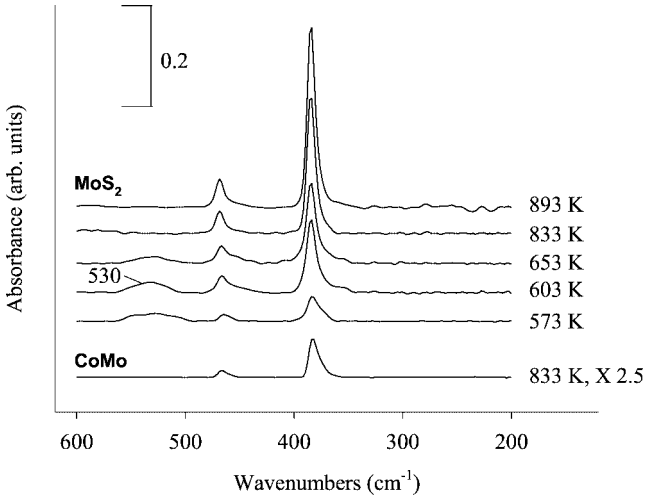

Figure 2. Far-IR spectra (600–200 cm^{-1}) of: unsupported MoS_{2+x} samples prepared by ATTM thermal decomposition under N_2 at different temperatures of treatment (upper part) and of Co/MoS_2 prepared in the same conditions at 833 K (lower part). Conditions: heating rate 2.5 K min^{-1}, 2 h at temperature T, N_2 flow 60 cm^3/min.

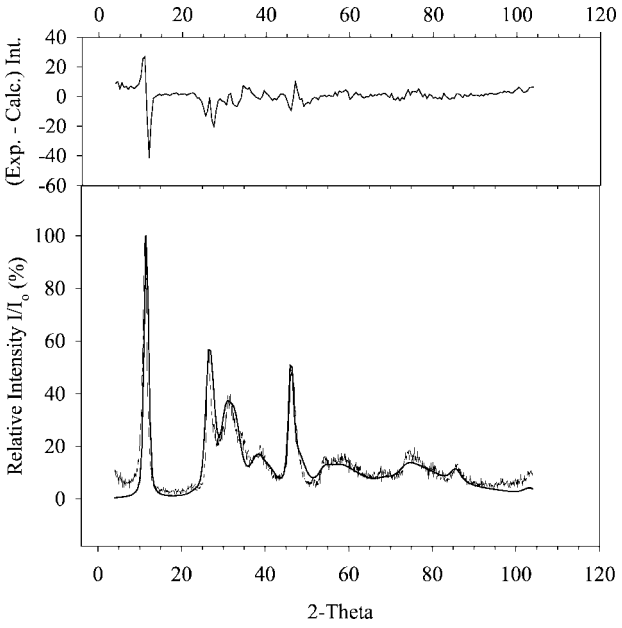

Figure 3. Comparison between experimental and simulated synchrotron XRD patterns of an MS833 sample (MoS_2 prepared from ATTM under N_2 at 833 K, 2 h). The upper graph represents the difference between these two patterns.

3.2. Synchrotron X-ray diffraction

Further insight regarding the structure of MoS_2 poorly crystalline samples was obtained using the SSRL (Stanford Synchrotron Radiation Laboratory) X-ray source. The powder diffractometer operating with an intense monochromatic beam ($\lambda = 1.2389$ Å) was used to record the XRD pattern of an MS833 (MoS_2 833 K ATTM decomposition in N_2) sample. The higher resolution and superior signal to noise of this technique was readily apparent. As reported in figures 3 and 4, MoS_2 and Co/MoS_2 diffractograms are typical of a poorly crystalline MoS_2 phase [21] with the most intense peak at $2\Theta = 11.2°$ ($\lambda = 1.2389$ Å) and a broad envelope beginning approximately at 25° and continuing above $2\Theta = 45°$ and characterized by the asymmetric shape of the (100) diffraction peak at $2\Theta = 26.5°$. This experimental pattern was fitted to a simulated pattern using the *Crystal Diffraction* and *Crystal Builder* modules from Cerius^2 4.0 (Molecular Simulations Inc.). Figure 3 reports the fitting results between experimental and simulated patterns as well as the difference of the two spectra (upper part). Quite satisfactory fitting was obtained using the 3R-MoS_2 crystallographic structure instead of a 2H-MoS_2 structure (space group: R3m unit cell dimensions: $a = 3.16$ Å, $c = 18.42$ Å). At low angles, the background presents a relatively high non-Bragg scattering. This is due to a highly disordered structure ("rag structure") in which individual MoS_2 layers are randomly folded and connected to each other. Additionally, the difference in the experimental and the calculated pattern for the (002) peak was attributed to preferential orientation. Moreover, on standard XRD patterns, it should be noted that the low-angle non-Bragg scattering signal disappears after a treatment at 893 K (not shown here) compared with the 833 K treatment. This shows that the disorder due to randomly folded layers is reduced. Meanwhile, the asymmetric shape of the (100) peak at $2\Theta = 34°$ peak still remains, indicating the presence of turbostratic MoS_2 (random layer lattice) which is typical of molybdenum-sulfide-based catalysts. A Rietveld refinement study confirmed the assignment of our starting material to a 3R structure. Starting from a 50% 3R–50% 2H mixed contribution in the experimental pattern, the best refinement gave a 94% 3R–6% 2H result. This 3R assignment was already observed starting from $(NH_4)_2MoS_4$ [22]. To distinguish between the 3R (rhombohedral) and 2H (hexagonal)-MoS_2 structures is quite difficult with standard XRD techniques and the quality of the synchrotron source is thus strikingly seen. Indeed, the two crystallographic structures are differing only in the layer sequence. In the 2H stacking sequence, compared to the first layer, the second layer is slightly shifted along the *a* axis from the first layer while the third one will be in the same atomic position. In the 3R sequence, only the fourth layer will be in the same atomic positions as the first one. From a catalytic point of view, the consequence of this slight difference is unknown. According to the "rim-edge" model [23], this different layer arrangement could probably induce some changes in selectivity.

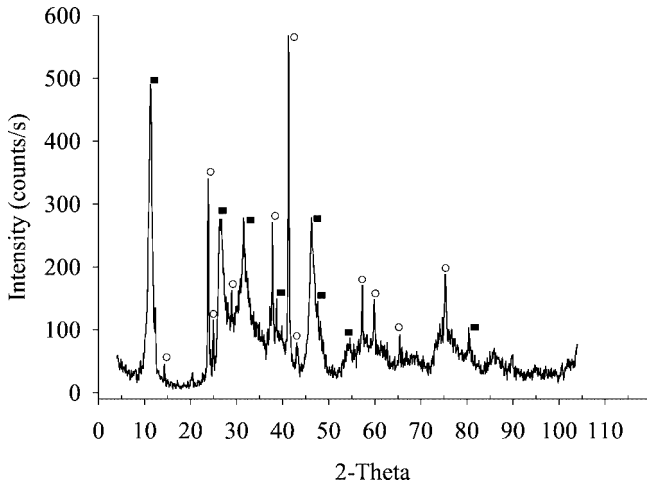

Figure 4. Synchrotron XRD pattern of a CMS833 sample (treatment under N_2 at 833 K, 2 h from Co/ATTM precursor). (■) MoS_2, (○) Co_9S_8.

Figure 4 reports the synchrotron XRD pattern of the CoMo sample after N_2 treatment at 833 K (CMS833). Apart from the diffraction peak characteristic of a poorly crystalline MoS_2 phase, quite intense peaks corresponding to Co_9S_8 are observed at 23.8° (311), 37.8° (333), 41.3° (440), 57.3° (731) + (553), 59.9° (800) and 75.3° (844). As expected from the lesser stability of the promoted catalysts, the high temperature of treatment (833 K) is responsible for the segregation of the Co/MoS_2 catalyst into their respective monosulfide phases, *i.e.*, MoS_2 and Co_9S_8 [24].

3.3. Thermal treatment with dimethyl sulfide

A real industrial hydrotreating unit is a triphasic reactor with a solid catalyst, hydrogen gas and a liquid phase com-

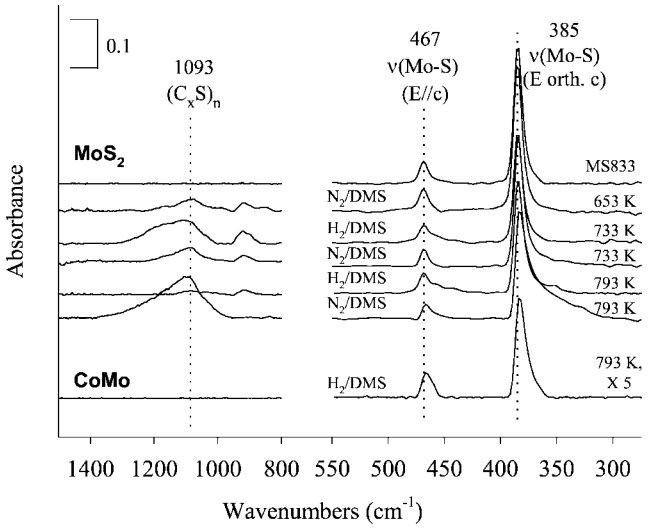

Figure 5. Evolution of the IR spectra of cobalt-promoted (lower part) and unsupported MoS_2 (upper part) samples recorded at different temperatures of DMS treatment under a N_2 (or H_2) atmosphere in the mid-IR wavenumber region (1400–800 cm^{-1}) and in the far-IR region (550–300 cm^{-1}).

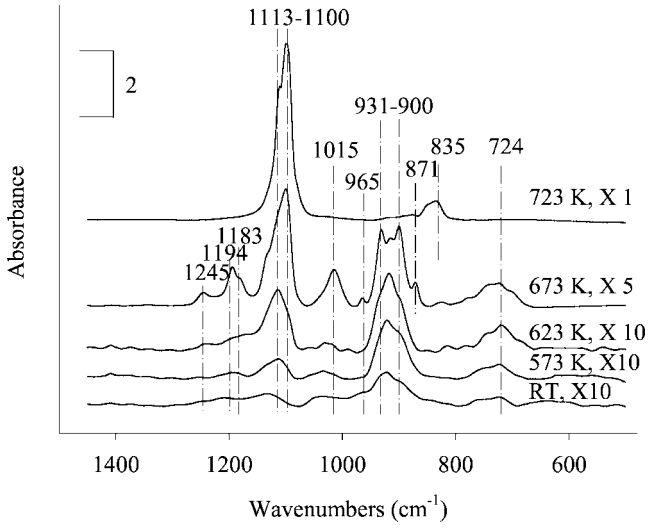

Figure 6. Evolution of the IR spectra in the 1450–600 cm^{-1} region of an MS773 sample heated in a closed IR cell in the presence of DMS (P_{DMS} = 10 Torr) at different temperatures of treatment after an evacuation at moderate vacuum (10^{-3} Torr).

posed of a complex mixture of hydrocarbons. Hydrogen must diffuse from the gas phase to the liquid one, solubilize, and then diffuse from the liquid phase to the catalyst surface before undergoing a dissociative chemisorption step, a prerequisite to the C heteroelement hydrogenolysis [25]. Therefore, two different dimethylsulfide treatments using nitrogen or hydrogen atmosphere were used in order to clarify the interaction of H_2 (or N_2) with DMS during the thermal treatment.

3.3.1. Infrared characterization after treatment under a DMS flow (dynamic mode)

Figure 5 reports the evolution of IR spectra recorded at different temperatures of DMS treatment under N_2 or H_2 atmospheres. A decrease of the intensity of the 385 cm^{-1} signal is observed as the temperature of treatment is increased. Moreover, the two Mo–S stretching bands gradually exhibit an asymmetric shape at lower wavenumbers. In the mid-IR region, intermediary products of the DMS decomposition as $(C_xS)_n$ polymer species are characterized by a broad band at 1093 cm^{-1} as well as a minor signal at 830 cm^{-1} [26]. As the N_2 temperature increases, these peaks are more intense indicating a further production of polymeric species. Using hydrogen at high temperature removes these $(C_xS)_n$ moieties for both unpromoted and cobalt-promoted samples.

3.3.2. Infrared characterization by direct in situ CH_3–S–CH_3 decomposition (static mode)

A 100 mg CsI pellet with 1 w% of MoS_2 was heated at 2 K min^{-1} in the presence of 10 Torr of CH_3–S–CH_3 up to a given temperature T and maintained 1 h at this temperature. The sample was then cooled down to RT before evacuation at moderate vacuum in a first step (10^{-3} Torr) before a complete evacuation at 10^{-6} Torr 2 h. Spectra were recorded without any contact with air and the mid-IR region was investigated. Figure 6 presents the spectra in the 1450–600 cm^{-1} wavenumber region for an MS773 sample (MoS_2 773 K ATTM decomposition in N_2). The C–S–C "skeleton" gives rise to absorption bands due to the ν(CSC) stretching modes between 780 and 690 cm^{-1} [27,28]. The methyl groups exhibit rocking modes of vibration at 1015, 965 and between 930 and 870 cm^{-1}. The $\delta(CH_3)$ bending modes at 1464, 1408 and 1345 cm^{-1} as well as the $\nu(CH_3)$ stretching bands at 2915 and 2986 cm^{-1} are very weak. Harmonic bands combining rocking modes and bending modes of the C–S–C skeleton are detectable at 1245, 1194 and 1182 cm^{-1}. A strong peak is also observed around 1100 cm^{-1} with a shoulder at 1113 cm^{-1} and is assigned to a ν(C=S) vibration [26]. The intensity of the peaks due to the CH_3–S–CH_3 adsorption increases as far as a temperature of treatment of 673 K. The 723 K treatment involves the disappearance of any peaks due to a CH_3–S–CH_3 adsorption, only the high intense ν(C=S) band is still present with a minor contribution at 835 cm^{-1}. The gas phase spectrum clearly showed the formation of methane. All the vibrations due to the CSC skeleton or due to methyl groups have completely vanished. These results showed that, in the absence of H_2, CH_3–S–CH_3 adsorbed irreversibly on the MoS_2 surface up to 673 K while, between 673 and 723 K, the DMS species decompose and only the formation of "carbosulfide" polymer species is detectable.

3.4. Electron energy loss spectroscopy (EELS)

EELS spectra records the scattered intensity of an electron beam passing through a target compound as a function of the decrease in kinetic energy. Repulsion from inner or outer shell atomic electrons of the analyzed sample provokes an inelastic scattering for the transmitted electrons at high-energy loss and low-energy loss values, respectively. For

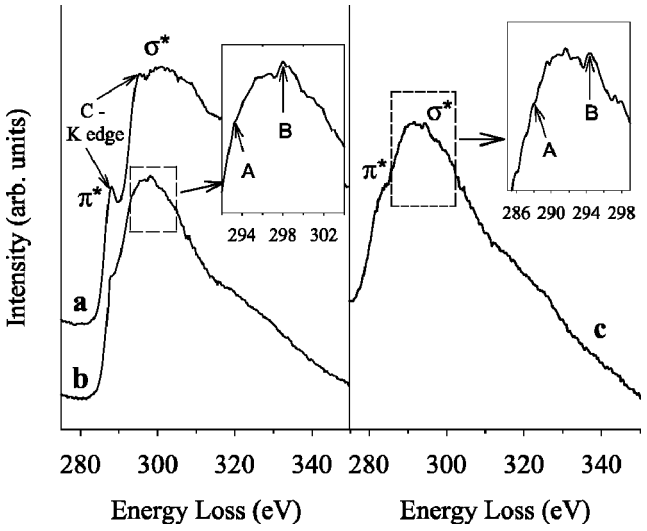

Figure 7. EELS C K-edge shapes (280–340 eV) of (a) a β-Mo_2C reference, (b) an MS833 sample treated at 793 K with N_2/DMS at a DMS partial pressure of 180 Torr (24.0 kPa) and (c) a CMS833 sample treated in the same conditions as (b). The inset presents the fine structure shape observed at the σ^* transition.

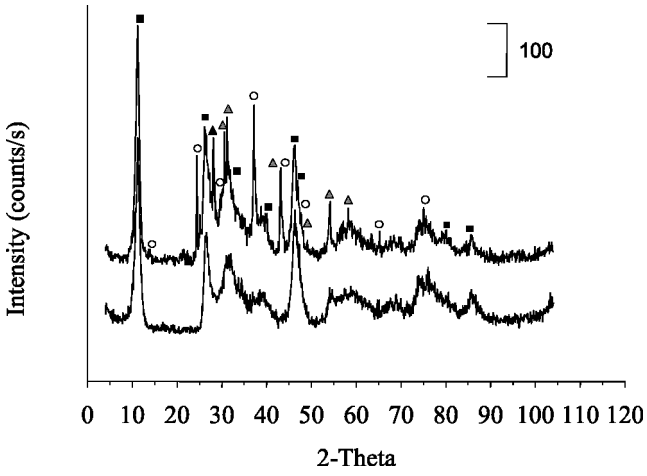

Figure 8. Comparison between the synchrotron XRD patterns of an MS833 sample and a CMS833 sample, both treated at 793 K with N_2/DMS at a DMS partial pressure of 180 Torr (24.0 kPa). (■) MoS_2, (○) Co_9S_8 and (△) Mo_2C.

inner-shell excitation, scattering is characterized by edges whose energy-loss values correspond to the binding energy of the atomic shell under consideration. The intensity of this "ionization threshold" is related to a particular element. These ionization edges possess a fine structure reflecting the energy-band structure of the studied element. Thus, EELS C K-edge shapes can help in differentiating between various carbon structures. Figure 7 reports the EELS C K-edge spectra for a β-Mo_2C reference and for the MS833 and CMS833 samples, both treated at 793 K with DMS (180 Torr) diluted in N_2. Two transitions corresponding to the π^* and σ^* antibonding states can be observed. As reported previously [11], for amorphous carbon, the C K-edge presents a smooth shape without noticeable peaks for the π^* and σ^* states. For graphite and carbide, two features A and B are detectable in the σ^* region. Their relative intensities correspond to a different density of states [29]. In the graphitic structure, carbon sp^2 bonds imply that A is at higher intensity than B whereas, for a carbidic structure, carbon sp^3 bonds are related to a higher intensity of feature B compared to A. Analysis of the fine structure of both MS833 and CMS833 samples confirm that B is at higher intensity than A. Consequently, the carbon structure does not appear graphitic. The surface stucture reveals the presence of Mo–C bonds of a carbide-like structure. However, the π^* shape is smoother than for pure Mo_2C revealing that a part of the carbon is also of amorphous nature. The presence of amorphous carbon and the absence of an organized graphitic structure was checked previously by high-resolution electron microscopy (HREM) and near-edge X-ray absorption fine structure (NEXAFS) spectroscopy [11]. NEXAFS also undoubtedly revealed the formation of a carbide-like structure on the MoS_2 surface [11].

EELS results confirm the formation of metal–carbon bonds at the surface of unsupported MoS_2 and Co/MoS_2 catalysts after DMS treatment. Moreover, careful study of the C K-edge fine structure reveals that features A and B are shifted 6 eV downwards for the DMS-treated Co/MoS_2 samples compared to MoS_2. This suggests strongly a weakening of the Me–C bond strength in the DMS-treated CoMo sample, which could be related to the electronic donation from Co to carbon-coordinated Mo.

3.5. Synchrotron X-ray diffraction

Synchrotron XRD studies were performed to check if the carbide-induced modification of the DMS-treated unsupported MoS_2 and Co/MoS_2 catalysts is restricted to the outermost layers or if carburization occurs deeply inside the bulk structure. As reported in figure 8 (lower part), for the unpromoted catalyst, the XRD pattern is typical of a MoS_2 layered structure. No new peaks are detected. However, careful analysis reveals that the intensity of the (110) plane at $2\Theta = 47°$ is surprisingly higher than this one for the (100) plane. Using the *Crystal Builder* and *Crystal Diffraction* modules from Cerius^2 4.0 (Molecular Simulations Inc.), fitting calculations between experimental and simulated patterns showed that this more intense (110) peak could be ascribed to a higher distortion (more folding) of the layered structure along the *c* axis following the DMS treatment. A quite different pattern was observed for the cobalt-promoted MoS_2 catalyst (upper part, figure 8). As already observed in figure 4, treatment at 833 K involves a phase segregation of the MoS_2 and Co_9S_8 phases. However, diffraction peaks of the Co_9S_8 phase are less intense than on the non-DMS treated CoMo catalyst. This suggests that crystallization of the cobalt sulfide phase is slightly retarded by the DMS treatment. This could be related to a retardation effect of amorphous carbon on the crystallization of sulfide phases [30,31]. Moreover, even if the intensity of the (110) plane remains important, the ratio $I(110)/I(100)$ somewhat decreases suggesting a slightly less bending effect on the remaining MoS_2 phase. More interestingly, new diffraction

peaks corresponding to a Mo_2C-like hexagonal phase appear. Indeed, molybdenum carbide peaks are observed at $2\Theta = 28.1°$ (100), 30.6° (002), 31.2° (101), 43.0° (102), 54.2° (103) and 58.4° (112) + (201). A diffraction peak corresponding to the (110) plane is expected at $2\Theta = 48.6°$ but is overlapped by the intense (110) diffraction peak of the MoS_2 phase. This result demonstrates that cobalt promotion has a strong influence on the degree of carburization of the MoS_2 phase when contacting to an organosulfide agent.

4. Discussion

In our previous studies [5,11], we have evidenced that carbon plays an important role in hydrotreatment modifying structurally the nature of the stabilized active phase in real hydrotreating conditions. This fact has pushed us to explore the consequences of the interaction of carbon-containing sulfiding agents with transition metal sulfides. Indeed, it is well known that organosulfide agents (CH_3–S–CH_3, CH_3–S–S–CH_3, alkylpolysulfides, *etc.*) improve activity of the final active phase [12]. Previous studies as well as the present one, through surface sensitive techniques, showed that the surface species present on MoS_2 and Co/MoS_2 catalysts are not only coordinately unsaturated sites (CUS), sulfhydryl (SH), S^{2-} or S_2^{2-} entities but also carbon moieties with a carbidic nature. However, the extent of this carburization effect is unknown at this point. Results obtained by Oyama and co-workers [15,16] demonstrated that the catalytic comportment of molybdenum carbide catalysts in hydrodesulfurization reactions tends to a final "carbosulfide" phase. It should be reasonably envisaged that the surface concentrations of the different species will reach an equilibrium between sulfur and carbon entities depending on reaction conditions. Otherwise, for similar conditions of treatment, we already obtained information for unsupported MoS_2 catalysts. IR molecular simulations were performed using the *Force-Field* and *IR/Raman* module of Cerius^2 4.0 (MSI Inc.). These fitting simulations were based on direct approximate calculations and not on density functional techniques (DFT) even if former DFT studies [32] were taken into account in order to first refine the MoS_2 crystallographic structure and secondly to build a definite 60 Å length model slab. Considering as observed by DFT only slight relaxation processes on the edges of MoS_2 slabs, our model fits well experimental Mo–S stretch frequencies at 385 and 467 cm^{-1}. As for oxidation reactions, a "cherry" model was then assumed with carburization progressing from the edges to the bulk of the model slab. Results showed that the asymmetric tail observed on IR spectra of DMS-treated MoS_2 samples is partly a result of carbon replacement of surface sulfur atoms through a topotactic process and/or bending of the layers. This topotactic process was already observed by Lee *et al.* [33] in a study about the α-MoC_{1-x} formation from MoO_3. HREELS experiments have indicated that the Mo–C stretching mode of vibration gives rise to signals in the 360–380 cm^{-1} wavenumber range [34]. However, no ν(Mo–C) signal was detectable in our β-Mo_2C IR spectra due to the Mo–Mo metallic interaction of this compound. In the present case, the detection of a ν(Mo–C) signal would be due to the fact that the carbide phase is supported on a MoS_2 bulk structure, well known to possess semiconducting properties [35]. More interestingly, these results confirmed that for MoS_2, the carburization replacement process is a surface reaction occurring only at the edges of MoS_2 slabs without progressing inside the bulk structure. A more advanced carburization effect will probably provoke phase segregation into MoS_2 and Mo_2C and is unrealistic considering temperature ranges.

As already mentioned, Boudart and co-workers [33] showed that molybdenum carbide synthesis from MoO_3 can occur through a topotactic process in which the synthesized metastable α-MoC_{1-x} phase exhibits pseudomorphism with the original platelets of MoO_3. A similar process can be envisaged in the present case. Morphological consequences of the formation of a carbosulfide phase could be approached through the formation of a mixed C–Mo–S sandwich layered structure. In a first step, the Mo_2C structure was built based on a hexagonal close-packed configuration of Mo layers with carbon in octahedral holes. A simulated XRD pattern was calculated and compared to literature data [36]. A quite good agreement is found with main peaks at 34.5°, 38.0°, 39.6°, 52.2°, 61.9° and 75.9° corresponding, respectively, to the (100), (002), (101), (102), (110) and (201) reflections. Next, an interface along the (001) planes of Mo_2C and MoS_2 was constructed. Surface cleavage along the (001) Mo_2C and MoS_2 planes exhibit a very similar configuration, as shown in figure 9. Indeed, angles and nonmetal–nonmetal distances

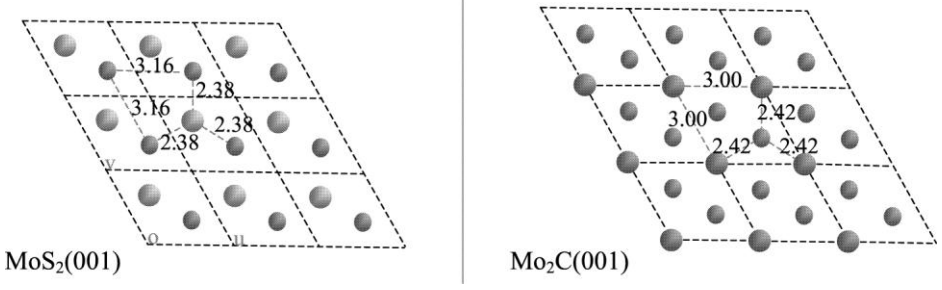

Figure 9. Comparison of the two (001) surface cleaved MoS_2 and β-Mo_2C. C(S)–Mo and C(S)–C(S) distances are indicated. Left side: Mo (small circles), S (large circles); right side: Mo (small circles), C (large circles). Metal–metal and sulfur (resp. carbon)–metal distances are indicated in Å.

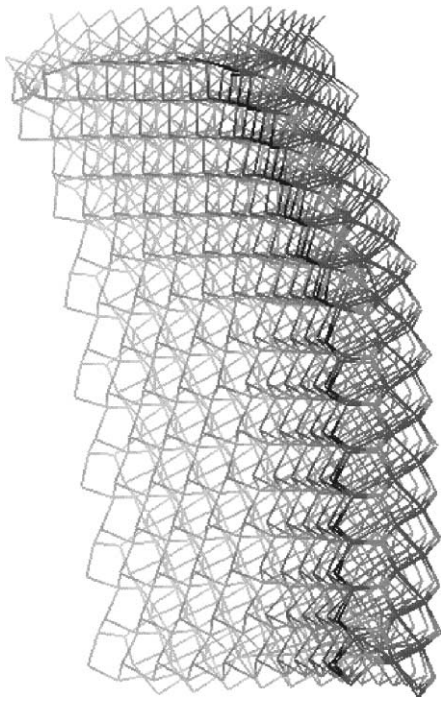

Figure 10. Example of a 40 Å × 40 Å MoS_2(001)–Mo_2C(001) interface after energy minimization (1500 iterations). A strong bending effect is observed with convexity on the sulfur side.

are quite close with a C–C distance of 3.00 Å and a S–S distance of 3.16 Å. The underlying Mo layer is at the center of a prism with a distance to the nearest nonmetal atoms of 2.42 and 2.39 Å, respectively, to carbon and sulfur. Therefore, the as-built interface along their respective (001) planes shows a good matching between C and S. The total energy of the Mo_2C–MoS_2 interface was minimized in order to determine the morphological consequences of the formation of a mixed C–Mo–S sandwich. As reported in figure 10, a strong bending effect is observed. In this particular case of a 40 Å × 40 Å interface, the bending angle reaches a value of 18°. This is in good agreement with previous results showing that MoS_2 nanotubes with lower diameter than 10 nm are energetically highly improbable due to strong strain forces on the Mo–S bond [37]. In this particular case, the curving radius would be 13 nm. As a matter of fact, fitting calculations on XRD results have also indicated a higher folding for DMS-treated MoS_2. However, this simulation does not correspond to a real modification of the particle shape. A so asymmetrical carburization process progressing only along one of the two S layers of the S–Mo–S sandwich without any replacement on the other side seems difficult to envisage. Nevertheless, as observed through the experimental results, a cherry model is acceptable with only replacement of sulfur atoms by carbon along the first outermost rows of the particle whereas the bulk structure remains sulfidic by nature. This effect has also been observed when an H_2/H_2S activated MoS_2 exfoliates in high vacuum in the presence of residual carbon [5,38]. This high reactivity of the MoS_2 edges *versus* carbon was also observed in previous results [39] and calculations on bent MoS_2 particles have recently been investigated [37]. These bent extremities suggest that the carbon replacement process occurs only along the MoS_2 edges and does not interfere with inner Mo rows. The bending consequence of the formation of this C–Mo–S sandwich would be related to a slightly smaller Mo–S distance compared to the Mo–C one; indeed, the bending curve appears convex on the sulfur side. Thus, a part of the asymmetric shape observed for the IR peaks corresponding to Mo–S stretching modes could be due to this folding effect. This experimental curved shape of the MoS_2 edges would signify that the C replacement process does not progress so symmetrically on each side of the S–Mo–S trilayer with probably a more advanced carburized effect on the "rim sites" [23] situated at the extremities of the stacked MoS_2 layers. However, the bending morphological consequences of the carbon inclusion could participate in a certain extent in the formation of less stacked and smaller crystallites after DMS treatment through exfoliation as already observed in some regions of electron micrographs. Indeed, as reported before [11], the DMS interaction could reduce by a factor of two stacking and particle size.

For cobalt-promoted MoS_2 catalyst, EELS, IR and XRD results confirm a carburization effect similar to this one observed for non-promoted MoS_2. However, XRD results suggest that cobalt promotion involves a higher tendency to carburize. This could be related to the higher reducibility of CoMo compared to MoS_2. Indeed, temperature-programmed reduction (TPR) results have shown that cobalt-promoted MoS_2 phase can be reduced more easily than the unpromoted phase for temperatures higher than 650 K [40]. This property was ascribed to the well-known electronic origin of promotion since in the CoMoS phase, Co donates electron to Mo weakening the Mo–S bond strength. In this way, cobalt promotion will favor indirectly carburization through electronic donation, resulting in higher reducibility of the Mo–S moieties. However, it is worth mentioning that at temperatures commonly used in hydrotreating reactions (623 K), both cobalt-promoted and unpromoted MoS_2 phases present similar degrees of reduction [40,41]. This supports that for this temperature range the carbide-like molybdenum phase is still engaged into a CoMo entity. Reducibility would simply help in carburizing molybdenum and will favor a more carbidic nature of Mo when involved into a Co–Mo electronic interaction. Consequently, the CoMoS phase initially present could be considered as a precursor phase leading under hydrotreating conditions to a CoMoC entity for which Co favors the carburization process. However, the case described here is a limiting case. In the hydrotreatment process, many experimental parameters (nature of hydrocarbons, temperature or pressure of treatment, partial pressure of the different reactants) could influence the surface state. It appears reasonable to say that the surface could vary from a partly to a completed carbided nature.

If reducibility appears a key parameter in the carburization process, one basic question arises: which mechanism is involved in this reaction? IR results suggest a possible explanation. First of all, as observed in figure 5, if H_2 is not used or is insufficiently present, polymer species are

Table 1
Mo, S and C contents of different unpromoted MoS_2 samples treated in the presence of 180 Torr (24.0 kPa) of CH_3–S–CH_3 with a H_2 atmosphere. Sulfur wt% was corrected to take into account overestimation of sulfur content. The correction was made by comparison to a reference: a highly crystallized MoS_2 sample with a S/Mo ratio of 2.00

Initial sample	Treatment	Mo (%)	S (%)	C (%)	Stoichiometry
MoS_{2+x}	N_2 at 833 K, 2 h	58.61	42.02	–	$MoS_{2.04}$
MoS_{2+x}	N_2 at 833 K, 2 h followed by H_2/DMS 793 K 180 Torr (24.0 kPa)	60.77	39.67	1.64	$MoS_{1.82}C_{0.22}$
$(NH_4)_2MoS_4$	Directly H_2/DMS 793 K 180 Torr (24.0 kPa)	61.31	39.11	1.50	$MoS_{1.80}C_{0.20}$

formed by degradation of $(CH_3)_2S$ species, probably initially coordinately bonded to the MoS_2 surface, as observed by Ziolek *et al.* [28]. These $(C_xS)_n$ entities are probably a "dead-end" product, which partly hampers the carburization process. Oppositely, as observed in the gas phase, in the presence of hydrogen, methane is one of the main products of the CH_3–S–CH_3 decomposition. Produced from $(CH_3)_2S$ species already linked to the surface, this nascent CH_4 could interact efficiently with surface species. As a matter of fact, the H_2/CH_4 reactant mixture is commonly used for reducing and carburizing MoO_3 precursor [42].

As shown in table 1, in the case of the unpromoted phase, similar final stoichiometries are obtained either starting from the thiosalt precursor, $(NH_4)_2MoS_4$ (Mo^{VI}) or from MoS_{2+x} (mainly Mo^{IV}). Even if the final temperatures of DMS treatment differs by 40 K, only few modifications could be expected between the two stoichiometries of the carburized samples due to this parameter alone. However, even taking into account this, the amount of structural carbon seems equivalent whatever the initial oxidation state of molybdenum. Even if we cannot rule out a possible role of hydrocarbons produced from DMS in the reduction of Mo, this would not be a crucial point in achieving the final active phase; bulk MoS_2 is thermodynamically more stable than bulk Mo_2C. On the other hand, previous results [5] have shown that a correlation exists between the overstoichiometric sulfur amount present in the initial state (*cf.* figure 1) and the final amount of structural carbon in the stabilized active phase. Even if the nature of the overstoichiometric sulfur is still in debate [43,44], studies suggest that these species would be terminal S_2^{2-} groups [45–47]. Moreover, while a quite distinct ν(S–S) signal was detected on MoS_{2+x} samples up to 673 K (*cf.* figure 2), after DMS treatment in this temperature range, we did not observe $(S–S)^{2-}$ groups anymore. This would suggest a possible redox interaction between terminal S_2^{2-} groups on the edges of MoS_2 layers and the nascent CH_4 produced from the decomposition of coordinately bonded DMS, preferentially in the presence of hydrogen. A tentative mechanism could then be envisaged according to the following equations:

$$CH_3–S–CH_3 + 2H_2 \rightarrow 2CH_4 + H_2S \quad (1)$$

$$Mo(S^{2-})_y(S_2^{2-})_z + zCH_4 \rightarrow Mo(S^{2-})_y(C)_z + 2zH_2S \quad (2)$$

However, further studies are needed to sustain this proposed mechanism, mainly by determining decomposition products of the DMS–(Co)MoS_2 reaction. Moreover, if carburization proceeds more easily for cobalt-promoted system, the nature of the sulfur species replaced by carbon (S atoms linked only to Mo or S shared between Mo and Co) is still in question. It should also be noted that kinetics of decomposition will play an important role in attaining appropriate final active phase [6–8].

5. Conclusions

The anisotropic nature of the layered molybdenum sulfide structure confers quite different site reactivity as a function of sulfur unsaturation degree. While basal planes with completely saturated sulfur atoms are catalytically inert, edge sites are now well known to be the only potential sites for hydrotreating reactions. Furthermore, it has recently appeared that the stabilized active phase in real hydrotreatment conditions actually presents a surface carbidic-like nature which lead us to reconsider the role of carbon. In this respect, organosulfide agents are known to be beneficial for achieving better hydrodesulfurization activity. Consequently, the interaction of carbon with transition metal sulfides was reinvestigated through the potential influence of organosulfur compounds in the activation process of catalysts.

Results showed that dimethylsulfide interacts with unpromoted MoS_2 through a carbon replacement of sulfur atoms located at the edges of the layers while the inherent low reactivity of saturated sulfur atoms limits this process to a surface chemistry type reaction. Cobalt promotion induces a higher tendency of the molybdenum sulfide phase to "surface carburization". A possible link between reducibility of a given sulfide phase and its propensity to carbon replacement could thus be envisaged. For cobalt-promoted systems, the higher degree of carburization might be related to a higher reducibility of Mo atoms involved in the initial CoMoS phase resulting from the electronic promotion from cobalt. Finally, both using a hydrogen or nitrogen atmosphere with DMS led to the formation of surface carbidic species even if this process of formation would probably be favored by the presence of hydrogen.

Apart from structural considerations, morphological consequences of the DMS–MoS_2 based solids interaction were observed. Previous studies have shown that the DMS treatment, particularly in the presence of a nitrogen atmosphere, leads to better dispersed MoS_2 particles with smaller and less stacked crystallites dispersed on "fluffy" amorphous carbon. This amorphous carbon involves a retardation effect on the crystalline growth stabilizing the active phase. Molecular simulations, IR and XRD results suggest that carbon inclusion into the MoS_2 structure could also induce a higher

folding nature of the layers particularly at the edges (or in plane defects) and favor exfoliation process.

Finally, based on the proportionality observed between the overstoichiometric sulfur content in the initial sulfide phase and the final amount of structural carbon, a tentative mechanism was proposed based on an interaction of hydrocarbons produced from DMS and terminal $(S–S)_2^{2-}$ groups.

Acknowledgment

This work was supported by a grant from the Government Services Administration, the US Department of Energy "Gateway" Program, the Robert A. Welch Foundation, the National Science Foundation, ATOFINA and the General Electric Faculty for the Future Program.

References

[1] B.C. Gates, J.R. Katzer and G.C.A Schuit, *Chemistry of Catalytic Process* (McGraw-Hill, New York, 1979) ch. 5.
[2] R.J.H. Voorhoeve and J.C.M. Stuiver, J. Catal. 23 (1971) 228.
[3] A.L. Farragher and P. Cossee, in: *Proc. 5th Int. Congress on Catalysis*, ed. J.W. Hightower (North Holland, Amsterdam, 1973) p. 1301.
[4] H. Topsøe, B.S. Clausen, R. Candia, C. Wivel and S. Morup, J. Catal. 68 (1981) 433.
[5] R.R. Chianelli and G. Berhault, Catal. Today 53 (1999) 357.
[6] R.R. Chianelli and T.A. Pecoraro, US Patent 4 288 422 (1981).
[7] R.R. Chianelli and T.A. Pecoraro, US Patent 4 826 797 (1989).
[8] R.L. Seiver and R.R. Chianelli, US Patent 4 544 481 (1985).
[9] G. Alonso, V. Petranovskii, M. Del Valle, J. Cruz-Reyes, A. Licea-Claverie and S. Fuentes, Appl. Catal. A 197 (2000) 87.
[10] G. Alonso, M. Del Valle, J. Cruz-Reyes, V. Petranovskii, A. Licea-Claverie and S. Fuentes, Catal. Today 43 (1998) 117.
[11] G. Berhault, A. Mehta, A.C. Pavel, J. Yang, L. Rendon, M.J. Yácaman, L. Cota Araiza, A. Duarte Moller and R.R. Chianelli, J. Catal. 198 (2001) 9.
[12] H. Hallie, Oil Gas J. 80(48) (1982) 69.
[13] R. Prada Silvy, P. Grange, F. Delannay and B. Delmon, Appl. Catal. 46 (1989) 113.
[14] J. van Gestel, J. Leglise and J.-C. Duchet, J. Catal. 145 (1994) 429.
[15] B. Dhandapani, T. St. Clair and S.T. Oyama, Appl. Catal. A 168 (1998) 219.
[16] V. Schwartz, V. Teixeira da Silva and S.T. Oyama, J. Mol. Catal. A 163 (2000) 87.
[17] C.H. Chang and S.S. Chan, J. Catal. 72 (1981) 139.
[18] E.Z. Diemann, Z. Anorg. Allg. Chem. 432 (1977) 127.
[19] G.L. Schrader and C.P. Cheng, J. Catal. 85 (1984) 488.
[20] K.S. Liang, R.R. Chianelli, F.Z. Chien and S.C. Moss, J. Non-Cryst. Solids 79 (1985) 251.
[21] R.R. Chianelli, Int. Rev. Phys. Chem. 2 (1982) 127.
[22] H.P. Wang, P. Skeldon, G.E. Thompson and G.C. Wood, J. Mater. Sci. 32 (1997) 497.
[23] M. Daage and R.R. Chianelli, J. Catal. 149 (1994) 414.
[24] R.R. Chianelli, Catal. Rev. Sci. Eng. 26 (1984) 361.
[25] D. Letourneur, R. Bacaud, M. Vrinat, D. Schweich and I. Pitault, Ind. Eng. Chem. Res. 37 (1998) 2662.
[26] V.B. Krebs and G. Gattow, Z. Anorg. Allg. Chem. 338 (1963) 225.
[27] J.P. Perchard, M.T. Forel and M.L. Josien, J. Chim. Phys. 61 (1964) 645.
[28] M. Ziolek, O. Saur, J. Lamotte and J.-C. Lavalley, J. Chem. Soc. Faraday Trans. 90 (1994) 1029.
[29] M.M. Disko, C.C. Ahn and B. Fultz, *Transmission Electron Energy Loss Spectrometry in Materials Science* (Booknews Inc., Portland, OR, 1992).
[30] C. Glasson, Ph.D. thesis, University of Lyon, Lyon, France.
[31] G. Alonso, M. Del Valle, J. Cruz, A. Licea-Claverie, V. Petranovskii and S. Fuentes, Catal. Lett. 52 (1998) 55.
[32] P. Raybaud, J. Hafner, G. Kresse and H. Toulhoat, Surf. Sci. 407 (1998) 237.
[33] J.S. Lee, L. Volpe, F.H. Ribeiro and M. Boudart, J. Catal. 112 (1988) 44.
[34] B. Frühberger and J.G. Chen, J. Am. Chem. Soc. 118 (1996) 11599.
[35] P. Raybaud, J. Hafner, G. Kresse and H. Toulhoat, J. Phys.: Condens. Matter. 9 (1997) 11107.
[36] P.A. Aegerter, W.W.C. Quigley, G.J. Simpson, D.D. Ziegler, J.W. Logan, K.R. McCrea, S. Glazier and M.E. Bussell, J. Catal. 164 (1996) 109.
[37] R.R. Chianelli, G. Berhault, P. Santiago, D. Mendoza, A. Espinosa, J.A. Ascensio and M.J. Yácaman, Mat. Tech. Adv. Perf. Mat. 15 (2000) 54.
[38] C.B. Roxlo, H.W. Deckmann, J.H. Dunsmiur, A.F. Ruppert and R.R. Chianelli, Mater. Res. Soc. Symp. Proc. 82 (1987) 481.
[39] R.R. Chianelli, A.F. Ruppert, S.K. Behal, B.H. Kear, A. Wold and R. Kershaw, J. Catal. 92 (1985) 56.
[40] G. Berhault, M. Lacroix, M. Breysse, F. Maugé, J.-C. Lavalley, H. Nie and L. Qu, J. Catal. 178 (1998) 555.
[41] M. Breysse, G. Berhault, S. Kasztelan, M. Lacroix, F. Maugé and G. Pérot, Catal. Today 66 (2001) 15.
[42] J.S. Choi, G. Bugli and G. Djéga-Mariadassou, J. Catal. 193 (2000) 238.
[43] P.J. Mangnus, A. Riezebos, A.D. van Langeveld and J.A. Moulijn, J. Catal. 151 (1995) 178.
[44] G. Berhault, M. Lacroix, M. Breysse, F. Maugé, J.-C. Lavalley and L. Qu, J. Catal. 170 (1997) 37.
[45] J. Polz, H. Zeilinger, B. Müller and H. Knözinger, J. Catal. 120 (1989) 22.
[46] S.I. Kim and S.I. Woo, Appl. Catal. 74 (1991) 109.
[47] J.C. Duchet, E.M. van Oers, V.H.J. de Beer and R. Prins, J. Catal. 80 (1983) 386.